Journal of Power Sources 219 (2012) 253–257

Contents lists available at SciVerse ScienceDirect

Journal of Power Sources

journal homepage: www.elsevier.com/locate/jpowsour

Short communication

One-step hydrothermal synthesis of hexangular starfruit-like vanadium oxide for high power aqueous supercapacitors

Jie Shao [a,b], Xinyong Li [b], Qunting Qu [a,*], Honghe Zheng [a,*]

[a] School of Energy, Soochow University, Suzhou, Jiangsu 215006, China
[b] College of Chemistry, Chemical Engineering and Material Science, Soochow University, Suzhou, Jiangsu 215006, China

HIGHLIGHTS

- Hexangular starfruit-like vanadium oxide was prepared by a facile and cheap method.
- The assembly process of starfruit-like VO_2 was demonstrated.
- VO_2 exhibits excellent high power capability and good cycling stability.

ARTICLE INFO

Article history:
Received 5 April 2012
Received in revised form
22 June 2012
Accepted 16 July 2012
Available online 27 July 2012

Keywords:
Supercapacitor
Starfruit
Vanadium oxide
High power

ABSTRACT

Homogenous hexangular starfruit-like vanadium oxide was prepared for the first time by a one-step hydrothermal method. The assembly process of hexangular starfruit-like structure was observed from TEM images. The electrochemical performance of starfruit-like vanadium oxide was examined by cyclic voltammetry and galvanostatic charge/discharge. The obtained starfruit-like vanadium oxide exhibits a high power capability (19 Wh kg^{-1} at the specific power of 3.4 kW kg^{-1}) and good cycling stability for supercapacitors application.

1. Introduction

Lithium ion batteries and supercapacitors, the two major categories of energy storage and conversion systems, are progressing towards the direction of high energy and high power, which depend greatly on the electrochemical properties of electrode materials [1–3]. Two major strategies have been adopted to enhance the electrochemical performance of electrode materials. The first one is to develop nanostructured materials with extremely large effective surface area [1,4]. The second one is utilizing the synergic effect of nanocomposites by combining a high-energy material with another high-power material [5–12]. The former method is able to improve the intrinsic properties of a kind of material. Nanotubes [13], nanowires [14], nanosheets [15], meso- or macro-porous nanostructures [16,17], and hierarchical-structured hollow spheres [18] have been demonstrated to exhibit better electrochemical performance than their bulk counterparts. The synthesis procedures for these unique-morphology materials require easy operation, low cost, and high yield, which are favorable from the viewpoint of practical application.

Vanadium oxides, with the advantages of high energy density, low cost, and capability of fast charge–discharge, are promising candidate materials for both lithium ion batteries and supercapacitors [19–21]. Various vanadium oxides with unique structures have been synthesized, such as V_2O_5 nanowires [6], nanoribbons [22], nanosheets [23], and porous nanostructures [24,25], etc. In this work, a hexangular starfruit-like vanadium oxide was prepared for the first time by a one-step hydrothermal approach. The assembly process of starfruit-like structure was clearly demonstrated by the TEM images of incompletely assembled hexangular vanadium oxide. Starfruit-like vanadium oxide delivers a specific energy of 19 Wh kg^{-1} at the specific power of 3.4 kW kg^{-1}, manifesting its excellent high power capability for supercapacitors application.

* Corresponding authors. Tel./fax: +86 (0) 51267870203.
E-mail addresses: qtqu@suda.edu.cn (Q. Qu), hhzheng@suda.edu.cn (H. Zheng).

0378-7753/$ – see front matter © 2012 Elsevier B.V. All rights reserved.
http://dx.doi.org/10.1016/j.jpowsour.2012.07.045

2. Experimental section

Hexangular starfruit-like vanadium oxide (VO_2) was prepared by a one-step hydrothermal method. Briefly, 0.6 g ammonium metavanadate, 1 g poly(ethylene oxide)-block-poly(propylene oxide)-block-poly(ethylene oxide) copolymer (P123, molecular weight: 5800) and 8 ml formic acid were dissolved in 60 ml distilled water. The mixture was transferred to an autoclave and heated at 180 °C for 48 h. The resulting precipitate was centrifuged, washed several times with water and acetone, and dried at 40 °C overnight. The yield of vanadium oxide powder is about 0.42 g. Vanadium oxide was also prepared free of P123 for comparison, which is denoted as VO_2 (im). SEM was obtained by Philip XL30 operated at 25 kV. TEM was performed using a JEOL JEM-2010 transmission electron microscope. The specific surface area was measured according to the BET method using Micromeritics TriStar II apparatus with liquid nitrogen at 77 K. XRD pattern was collected using a Rigaku D/MAX-IIA X-ray diffractometer with Cu Kα radiation. The surface electronic states were investigated by X-ray photoelectron spectroscopy (XPS; Perkin–Elmer PHI 5000C ESCA, using Al KR radiation) and the binding energy values were calibrated using $C_{1s} = 284.6$ eV as a reference.

For electrochemical tests, the VO_2 electrodes were prepared by the following method. First, a thin film composed of a mushy mixture of VO_2, acetylene black (Shanghai Haohua Chemical and Industrial Co., Ltd.) and poly(tetrafluoroethylene) (PTFE, Sigma–Aldrich, 60 wt % dispersion in H_2O) in a weight ratio of 8:1:1 was prepared, and then punched into small disks with a diameter of 10 mm. At last, these disks were pressed onto a Ni-grid at a pressure of 12 MPa and then dried at 70 °C for 5 h. The active material on every electrode is about 4 mg cm^{-2}. 0.5 mol l^{-1} of K_2SO_4 aqueous solution was used as electrolyte. Electrochemical tests of the VO_2 electrodes were performed using a three-electrode cell, in which Ni-grid and saturated calomel electrode (SCE) were used as the counter and the reference electrode, respectively. Cyclic voltammetric (CV) data were collected between −0.1 and 1.0 V (*vs.* SCE) at different scan rates. Galvanostatic charge/discharge tests of VO_2 electrodes were performed in the potential range of 0–1.0 V.

From CV curves, the specific capacitance of VO_2 electrode was calculated based on the formula $C_s = \int IdU/2v \cdot m \cdot \Delta U$, where I is the current (A), $\int IdU$ is the integration area for the CV curve of VO_2 electrode, v is the scan rate (V s^{-1}), m is the mass (g) of the active material VO_2 in the composite electrode, ΔU is the potential window (V) during negative scan, and the factor 2 comes from the fact that the above integration area include both the positive scan and negative scan. The corresponding energy density (E_d) of VO_2 was calculated using the formula $E_d = 1/2C_sU_a^2$, where C_s is the specific capacitance (F g^{-1}), U_a is the average working potential (V *vs.* SCE) of VO_2 electrode. Here U_a is considered to be 0.5 V *vs.* SCE. The corresponding power density (P_d) of VO_2 was calculated using the formula $P_d = E_d/t$, where E_d is the energy density, t is the discharge time (h). During the CV scans, t is considered to the time period during the negative scan from 1.0 to 0 V *vs.* SCE.

From the charge/discharge curves, the specific capacitance was calculated using formula $C = I \cdot t/m \cdot \Delta U$, where I is the current (A) used for charge/discharge cycling, t is the discharge time (seconds), m is the mass (g) of the active VO_2 material, ΔU is the operating potential window (V) during discharge.

3. Results and discussion

SEM images of the vanadium oxide prepared in the presence of P123 (Fig. 1a and b) present a homogeneous hexangular starfruit-like morphology. The typical picture of starfruits is shown in Fig. 1c. The diameter of hexangular vanadium oxide ranges from 0.3 to 1.5 μm. The top-view of hexangular vanadium oxide observed from TEM image (Fig. 1d) exhibits a distinct hexangular shape, and the side-view of the six angles (Fig. 1e) presents a nanosheet structure with thickness of about 100–200 nm. The starfruit-like vanadium oxide has a specific surface area of about 56 m^2 g^{-1}

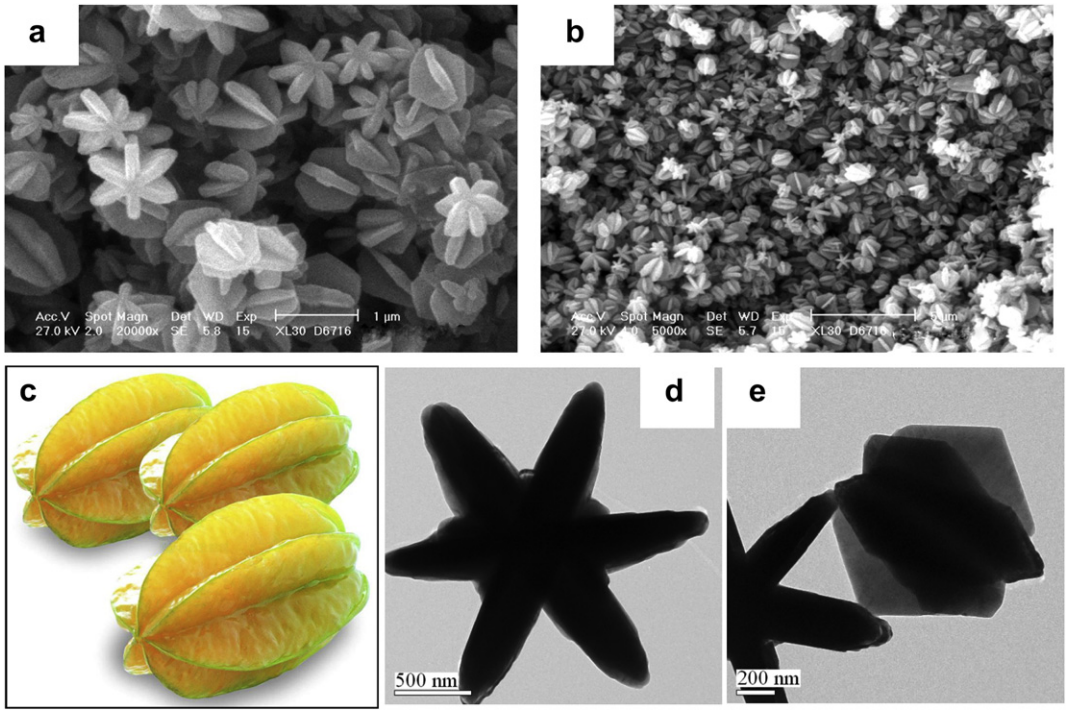

Fig. 1. SEM images of the vanadium oxide prepared in the presence of P123 at (a) high and (b) low magnification. (c) One typical picture of hexangular starfruits. (d and e) TEM images of hexangular vanadium oxide observed from top-view and side-view.

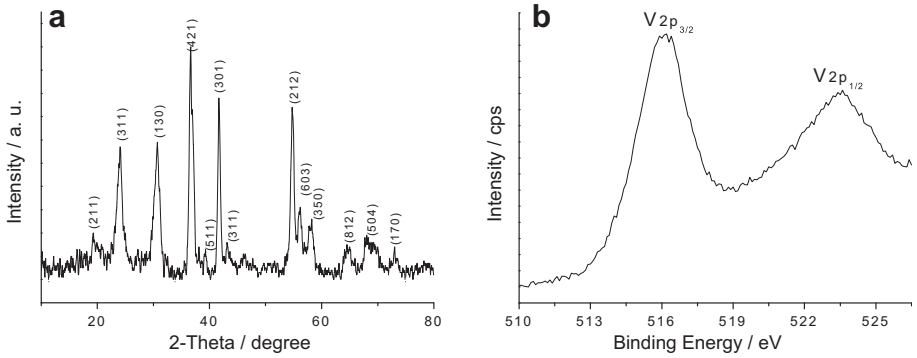

Fig. 2. (a) XRD pattern (b) XPS V_{2p} spectrum of the starfruit-like vanadium oxide.

measured by BET method and its XRD pattern (Fig. 2a) corresponds well to the characteristic diffraction peaks of V_xO_2 (JCPDF No. 34-0608). The color of V_xO_2 powder is dark blue, suggesting that V^{5+} was reduced to V^{4+} by formic acid during the hydrothermal treatment. The valence state of vanadium in the as-prepared product was further investigated through XPS. As can be seen from the XPS spectrum in the V_{2p} region (Fig. 2b), the binding energies of $V_{2p3/2}$ and $V_{2p1/2}$ are centered at 516.10 and 523.50 eV, respectively, in good accordance with the characteristic binding energies of V^{4+} [26]. Therefore, the starfruit-like vanadium oxide is denoted as VO_2 in the following part. The chemical equations for the formation of VO_2 are as follows.

$$2VO_3^- + 2H^+ \rightarrow V_2O_5 + H_2O \quad (1)$$

$$V_2O_5 + HCOOH \rightarrow 2VO_2 + H_2O + CO_2 \quad (2)$$

In order to understand the growth condition of hexangular starfruit-like VO_2, vanadium oxide was also prepared free of P123 for comparison, which is denoted as VO_2 (im). Its SEM image is shown in Fig. 3a. It can be seen that most of the products maintain a roughly hexangular structure but with some extra nanosheets and nanofibers distributed on the surface. The uniformity and stacking compactness of this material is not as good as that of starfruit-like VO_2 obtained in the presence of P123. These phenomena suggest that the acidic and reductive properties of formic acid lead to the growth of VO_2 nanosheets and nanofibers, and some of these nanofibers and nanosheets tend to self-assemble into hexangular structure, which was clearly demonstrated by one TEM image of incompletely assembled vanadium oxide prepared free of P123 (Fig. 3b). We can see that these nanosheets and nanofibers stack together in a unique manner with nanosheets located in the center and nanofibers sticking out towards the periphery in six directions. However, there are still many randomly dispersed nanofibers and nanosheets for the materials prepared without P123 (see Supporting information). In the presence of P123, the surfactant P123 is distributed on the surface of these nanofibers and nanosheets, making them assemble or cross-linked together in a more compact and perfect manner, thus giving rise to the uniform starfruit-like structure.

CV curves of starfruit-like VO_2 electrodes in 0.5 mol l^{-1} K_2SO_4 aqueous electrolyte at various scan rates are shown in Fig. 4a. Although there are no distinct redox peaks, the shape of the CV curves deviates from the ideal rectangle, indicative of the faradic pseudocapacitive nature of VO_2. The specific capacitance of starfruit-like VO_2 calculated from CV curves at the scan rate of 5 mV s^{-1} is 218 F g^{-1} (Fig. 4b), close to or higher than the reported capacitance of porous V_2O_5, high surface area V_2O_5, and electrospun V_2O_5 nanofibers [25,27,28]. The specific capacitance of acetylene black at various scan rates is also shown in Fig. 4b for comparison. We can see that the capacitance contribution of acetylene black is negligible. Moreover, the VO_2 electrode displays an excellent high rate behavior with 69% of its initial capacitance maintained when the scan rate increases to 50 mV s^{-1}. The rate capability of VO_2 is comparable to that of V_2O_5/carbon nanofibers composites [29]. The corresponding specific energy is 27 Wh kg^{-1} at the specific power of 0.5 kW kg^{-1} and 19 Wh kg^{-1} at the specific power of 3.4 kW kg^{-1} (Fig. 4c), much higher than those of electrospun V_2O_5 nanofibers [28], V_2O_5/carbon nanofibers composites [29], and V_2O_5/exfoliated graphite composites [30]. In addition, the starfruit-like VO_2 materials prepared with P123 exhibit much better electrochemical performance than those prepared without P123. All these data indicate a high power capability of VO_2, which

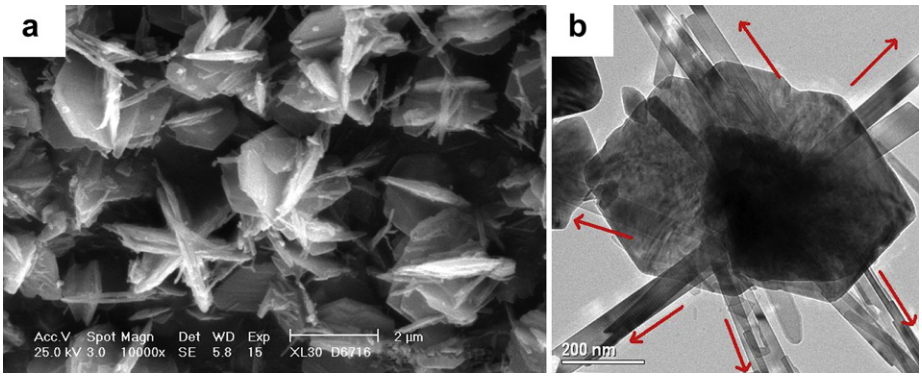

Fig. 3. (a) SEM image and (b) one TEM image of vanadium oxide prepared free of P123.

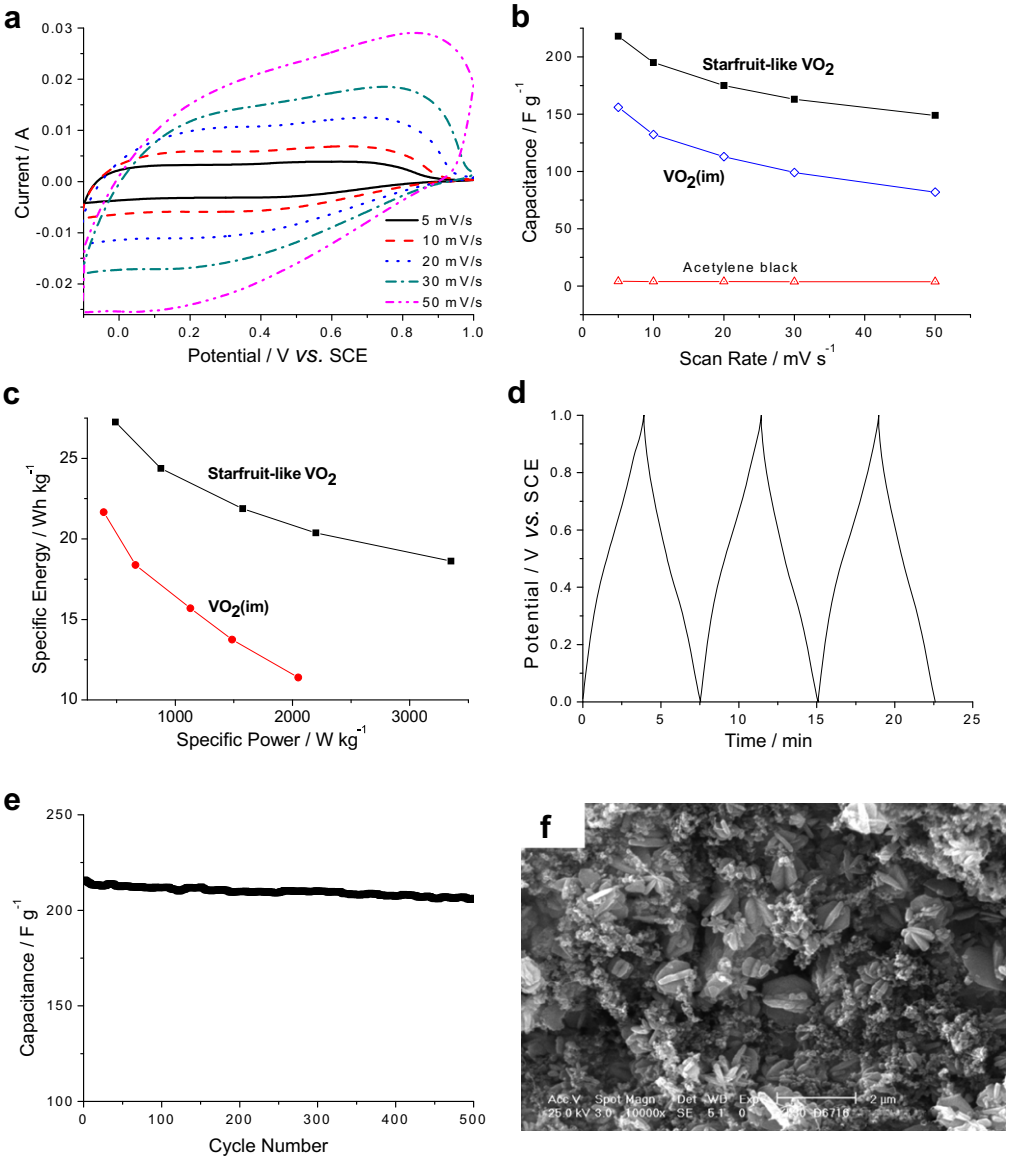

Fig. 4. (a) CV curves of starfruit-like VO_2 electrodes in K_2SO_4 aqueous electrolyte at various scan rates. (b) Specific capacitance of starfruit-like VO_2, VO_2 (im), and acetylene black as a function of scan rate. (c) Ragone plots of starfruit-like VO_2 and VO_2 (im). (d) Galvanostatic charge–discharge curves of starfruit-like VO_2 electrode at the current density of 1 A g^{-1}. (e) Cycling performance of starfruit-like VO_2. (f) SEM image of the VO_2 electrode after electrochemical cycles.

must be related to its unique starfruit-like nanostructure. The interstices between the six angles of starfruit-like structure can provide a large space to accommodate the electrolytes and conductive additives, thus facilitating the transport of both ions and electrons.

The galvanostatic charge/discharge curves of VO_2 electrode in K_2SO_4 aqueous electrolyte (Fig. 4d) exhibit an almost linear relationship with time, characteristic of the fast charge storage/release process of faradic pseudocapacitors. The reversible capacitance of VO_2 electrode at the current density of 1 A g^{-1} is 216 F g^{-1}, in good agreement with the CV results. It average working potential is up to 0.5 V *vs.* SCE, resembling to that of MnO_2 and RuO_2 materials [14,31]. The specific capacitance of VO_2 electrode during extended electrochemical cycles (Fig. 4e) maintains about 95% of its initial value after 500 cycles, signifying a good stability of VO_2 material. SEM image of the VO_2 electrode after electrochemical cycles (Fig. 4f) suggest that the hexangular starfruit-like structure of vanadium oxide was maintained rather well. The unique starfruit-like nanostructure may solve the aggregation problem of nano-scaled electrode materials during long-term cycles and improve their structural stability.

4. Conclusion

A hexangular starfruit-like VO_2 was prepared by a one-step hydrothermal treatment of NH_4VO_3, HCOOH, and P123 solutions. The primarily formed nanosheets and nanofibers tend to stack together in a special manner with the former located in the center and the latter sticking out towards the periphery in six directions. Tri-block copolymer P123 favors the assembly of these nanosheets and nanofibers in a compact and perfect manner, which accounts for the fabrication of homogeneous starfruit-like structure. The obtained VO_2 exhibits a high power capability and good stability for supercapacitors application attributed to its unique hexangular starfruit-like structure. In the future work, this type of starfruit-like VO_2 can also be applied to other energy storage systems such as

lithium ion batteries and solar energy cells, and employed as template for the synthesis of other special-structured functional materials.

Acknowledgments

Financial support from National Natural Science Foundation of China (NSFC No. 21073129) and The Natural Science Foundation of Jiangsu Province (BK2012186) is greatly appreciated.

Appendix A. Supplementary material

Supplementary material associated with this article can be found, in the online version, at http://dx.doi.org/10.1016/j.jpowsour.2012.07.045.

References

[1] J.R. Miller, R.A. Outlaw, B.C. Holloway, Science 329 (2010) 1637.
[2] P. Simon, Y. Gogotsi, Nat. Mater. 7 (2008) 845.
[3] H.-G. Jung, M.W. Jang, J. Hassoun, Y.-K. Sun, B. Scrosati, Nat. Commun. 2 (2011) 516.
[4] X.-L. Wang, W.-Q. Han, H. Chen, J. Bai, T.A. Tyson, X.-Q. Yu, X.-J. Wang, X.-Q. Yang, J. Am. Chem. Soc. 133 (2011) 20692.
[5] M.B. Sassin, C.N. Chervin, D.R. Rolison, J.W. Long, Acc. Chem. Res. (2012). http://dx.doi.org/10.1021/ar2002717.
[6] Z. Chen, V. Augustyn, J. Wen, Y. Zhang, M. Shen, B. Dunn, Y. Lu, Adv. Mater. 23 (2011) 791.
[7] Q. Qu, S. Yang, X. Feng, Adv. Mater. 23 (2011) 5574.
[8] H. Wang, L.-F. Cui, Y. Yang, H. Sanchez Casalongue, J.T. Robinson, Y. Liang, Y. Cui, H. Dai, J. Am. Chem. Soc. 132 (2010) 13978.
[9] Y. Sun, X. Hu, W. Luo, Y. Huang, ACS Nano 5 (2011) 7100.
[10] L. Buglione, M. Pumera, Electrochem. Commun. 17 (2012) 45.
[11] X. Zhu, H. Dai, J. Hu, L. Ding, L. Jiang, J. Power Sources 203 (2012) 243.
[12] W. Tang, Y.Y. Hou, X.J. Wang, Y. Bai, Y.S. Zhu, H. Sun, Y.B. Yue, Y.P. Wu, K. Zhu, R. Holze, J. Power Sources 197 (2012) 330.
[13] X. Lu, G. Wang, T. Zhai, M. Yu, J. Gan, Y. Tong, Y. Li, Nano Lett. 12 (2012) 1690.
[14] H. Jiang, T. Zhao, J. Ma, C. Yan, C. Li, Chem. Commun. 47 (2011) 1264.
[15] W. Tang, L. Liu, S. Tian, L. Li, Y. Yue, Y. Wu, K. Zhu, Chem. Commun. 47 (2011) 10058.
[16] T. Brezesinski, J. Wang, S.H. Tolbert, B. Dunn, Nat. Mater. 9 (2010) 146.
[17] Q. Qu, L. Fu, X. Zhan, D. Samuelis, J. Maier, L. Li, S. Tian, Z. Li, Y. Wu, Energy Environ. Sci. 4 (2011) 3985.
[18] L. Zhou, D. Zhao, X. Lou, Angew. Chem. Int. Ed. 51 (2012) 239.
[19] M. Sathiya, A.S. Prakash, K. Ramesha, J.M. Tarascon, A.K. Shukla, J. Am. Chem. Soc. 133 (2011) 16291.
[20] Z. Chen, Y. Qin, D. Weng, Q. Xiao, Y. Peng, X. Wang, H. Li, F. Wei, Y. Lu, Adv. Funct. Mater. 19 (2009) 3420.
[21] J.-M. Li, K.-H. Chang, C.-C. Hu, Electrochem. Commun. 12 (2010) 1800.
[22] Q.T. Qu, Y. Shi, L.L. Li, W.L. Guo, Y.P. Wu, H.P. Zhang, S.Y. Guan, R. Holze, Electrochem. Commun. 11 (2009) 1325.
[23] Z.-l. Wang, D. Xu, L.-m. Wang, X.-b. Zhang, ChemPlusChem 77 (2012) 124.
[24] Y. Yang, S.P. Albu, D. Kim, P. Schmuki, Angew. Chem. Int. Ed. 123 (2011) 9237.
[25] R.N. Reddy, R.G. Reddy, J. Power Sources 156 (2006) 700.
[26] X. Liu, G. Xie, C. Huang, Q. Xu, Y. Zhang, Y. Luo, Mater. Lett. 62 (2008) 1878.
[27] Z.J. Lao, K. Konstantinov, Y. Tournaire, S.H. Ng, G.X. Wang, H.K. Liu, J. Power Sources 162 (2006) 1451.
[28] G. Wee, H.Z. Soh, Y.L. Cheah, S.G. Mhaisalkar, M. Srinivasan, J. Mater. Chem. 20 (2010) 6720.
[29] A. Ghosh, E.J. Ra, M. Jin, H.-K. Jeong, T.H. Kim, C. Biswas, Y.H. Lee, Adv. Funct. Mater. 21 (2011) 2541.
[30] J.S. Bonso, A. Rahy, S.D. Perera, N. Nour, O. Seitz, Y.J. Chabal, K.J. Balkus Jr., J.P. Ferraris, D.J. Yang, J. Power Sources 203 (2012) 227.
[31] R.-R. Bi, X.-L. Wu, F.-F. Cao, L.-Y. Jiang, Y.-G. Guo, L.-J. Wan, J. Phys. Chem. C 114 (2010) 2448.